Intercomparison of in-situ NDIR and column FTIR measurements of CO_2 at Jungfraujoch

Michael F. Schibig[1], Emmanuel Mahieu[2], Stephan Henne[3], Bernard Lejeune [2], Markus C. Leuenberger[1]

[1] Climate and Environmental Physics, Physics Institute and Oeschger Centre for Climate Change Research, University of Bern, Bern, Switzerland

[2] Institut d'Astrophysique et de Géophysique, Université de Liège, Liège, Belgique

[3] Empa, Swiss Federal Laboratories for Materials Testing and Research, Dübendorf, Switzerland

Correspondence to: leuenberger@climate.unibe.ch

Keywords: CO_2, FTIR, NDIR, Jungfraujoch, intercomparison, CO_2 trend

Abstract

We compare two CO_2 time series measured at the High Alpine Research Station Jungfraujoch (3580 m a.s.l., Switzerland) in the period from 2005 to 2013 with an in-situ surface measurement system using a nondispersive infrared analyzer (NDIR) and a ground-based remote sensing system using solar absorption Fourier Transform Infrared spectrometry (FTIR). Although the two data sets show an absolute shift of about 13 ppm, the slopes of the annual CO_2 increase are in good agreement within their uncertainties. They are 2.04 ± 0.07 ppm yr^{-1} and 1.97 ± 0.05 ppm yr^{-1} for the FTIR and the NDIR system, respectively. The seasonality of the FTIR and the NDIR system is 4.46 ± 1.11 ppm and 10.10 ± 0.73 ppm, respectively. The difference is caused by a dampening of the CO_2 signal with increasing altitude due to mixing processes. While the minima of both data series occur in the middle of August, the maxima of the two datasets differ by about ten weeks, the maximum of the FTIR measurements is in middle of January, whereas the maximum of the NDIR measurements is found at the end of March. Sensitivity analyses revealed that the air masses measured by the NDIR system at the surface of Jungfraujoch are mainly influenced by central Europe, whereas the air masses measured by the FTIR system in the column above Jungfraujoch are influenced by regions as far west as the Caribbean and the United States.

1 The correlation between the hourly averaged CO_2 values of the NDIR system and the

2 individual FTIR CO_2 measurements is 0.820, which is very encouraging given the largely

3 different sampling volumes. Further correlation analyses showed, that the correlation is

4 mainly driven by the annual CO_2 increase and to a lesser degree by the seasonality. Both

5 systems are suitable to monitor the long-term CO_2 increase, because this signal is represented

6 in the whole atmosphere due to mixing.

8 1 Introduction

9 CO_2 is the most important anthropogenic greenhouse gas, with a large contribution to the

10 greenhouse effect (Arrhenius, 1896) and an additional radiative forcing of the atmosphere

11 currently evaluated at 1.68 Wm^{-2} (IPCC, 2013). The strength of the forcing is depending on

12 its atmospheric mole fraction which is ruled by the processes of the carbon cycle as well as by

13 anthropogenic CO_2 emissions from fossil fuel combustion and land use change. The major

14 reservoirs of the carbon cycle besides the lithosphere are the soils, the ocean, the biosphere

15 and the atmosphere, where the latter is also acting as the main link between the biosphere and

16 the ocean. The linking process between the atmosphere and the ocean is dissolution of CO_2 in

17 oceanic water, where it is subsequently chemically bound to bicarbonate and carbonate and

18 therefore removed from the carbon cycle on a longer timescale (Broecker and Peng,

19 1982;Feely et al., 2004;Heinze et al., 1991;Sillén, 1966). The processes coupling the

20 biosphere with the atmosphere are photosynthesis, where CO_2 is taken up by plants, and

21 respiration, where CO_2 is released back to the atmosphere. Photosynthesis and respiration are

22 mainly driven by climatic conditions of the environment. In the northern hemisphere,

23 especially in the extratropics with distinct seasons, the dominating process in late spring,

24 summer and fall is photosynthesis and thereby the uptake of CO_2 from the atmosphere. In

25 autumn respiration and with it the release of CO_2 from the biosphere into the atmosphere

26 starts to take over and is the ruling process in winter until spring when photosynthesis

27 becomes the dominating process again. Due to these alternating processes, the CO_2 mole

28 fraction in the atmosphere shows a seasonal cycle with its maximum generally in early spring

29 and its minimum in fall (Halloran, 2012;Keeling et al., 1976;Keeling et al., 2001;Machida et

30 al., 2002). A further component in the change of atmospheric CO_2 mole fraction is CO_2

31 release due to fossil fuel combustion (Karl and Trenberth, 2003;Revelle and Suess, 1957;Tans

32 et al., 1990). Nowadays, roughly half of the anthropogenically produced CO_2 ends up in the

oceans and the biosphere, whereas the other half is accumulating in the atmosphere and leads to a more or less steady increase of the atmospheric CO_2 mole fraction (Bender et al., 2005;Le Quéré et al., 2013;Sabine et al., 2004). Measuring the atmosphere's CO_2 mole fraction on the long-term is therefore important to understand the sources and sinks of the carbon cycle and the annual CO_2 increase due to fossil fuel combustion and land use change. To measure the evolution of CO_2 in the atmosphere on a global scale satellite remote sensing methods can be used as e.g. OCO-2 (Crisp et al., 2004, Pollock et al., 2010, Thompson et al., 2012) or GOSAT (Chevallier et al., 2009, Yokota et al., 2009) but they are limited by e.g. cloud cover, temporal coverage due to the orbit, coarse resolution etc. An intercomparison between GOSAT and several TCCON (Total Carbon Column Observation Network) stations showed a mean difference for daily averages of -0.34 ± 1.37 ppm (Heymann et al., 2015). Ground based measurement systems on the other hand have a high temporal resolution and provide very accurate data, which can be used to validate satellite data (Buchwitz et al., 2006; Butz et al., 2011;Dils et al., 2006; Morino et al., 2011;Wunch et al., 2011) or as model input (Chevallier et al., 2010), but surface observations have often a limited representativeness and are often influenced by nearby processes and hence, not representative for larger areas. Also the influence of the biosphere or anthropogenic pollution can be a serious issue and make it very challenging to measure background air. Therefore, to measure global CO_2 trends the sampling site should be at a very remote place like e.g. Mace Head Station (Bousquet et al., 1996;Messager et al., 2008) on the western coast of Ireland or the flask sampling network in the Pacific of NOAA (Komhyr et al., 1985;Trolier et al., 1996). Another possibility is to measure in the free troposphere e.g. with airplanes as done in the CARIBIC project (Brenninkmeijer et al., 2007) or the CONTRAIL project (Machida et al., 2008) or at high altitudes which are mostly in the free troposphere as e.g. Mauna Loa (Keeling et al., 1976;Keeling et al., 1995;Pales and Keeling, 1965;Thoning et al., 1989). The High Alpine Research Station Jungfraujoch (JFJ) with its altitude of 3580 m a.s.l. (Sphinx Observatory) and position mostly above the planetary boundary (Henne et al., 2010) is therefore a very suitable spot to conduct ground based CO_2 background measurements.

The University of Liège (Belgium) has been measuring infrared radiation at JFJ since the 1950s and started regular FTIR (Fourier Transform InfraRed) measurements in 1984. The Climate and Environmental Physics Division (KUP) of the University of Bern started measuring CO_2 and $\delta O_2/N_2$ in 2000 by a flask sampling program and since the end of 2004, CO_2 and O_2 have been additionally measured with a continuously operating system of a NDIR

1 instrument and a paramagnetic cell. In this study we compared the FTIR and the NDIR data

2 set to see if the two complementary measurement techniques are catching the same trends,

3 seasonalities and variations in atmospheric CO_2 mole fraction at and above Jungfraujoch.

2   Methods

2.1   Measurement site

7 The High Altitude Research Station Jungfraujoch (JFJ) is located 7°59'02'' E, 46°32'53'' N

8 at the northern margin of the Swiss Alps. The Jungfraujoch is a mountain saddle between the

9 Mönch (4099 m a.s.l.) and Jungfrau (4158 m a.s.l.) summits at a height of 3580 m a.s.l.

10 (Sphinx Observatory) and is accessible year-round by train. Because of the high elevation, the

11 station is usually above the planetary boundary layer (PBL) and therefore mainly receives air

12 from the free troposphere which is why it was classified as "mostly remote" by Henne et al.

13 (2010). Nevertheless, the station can be influenced by polluted air during specific events such

14 as frontal passages and Föhn (Uglietti et al., 2011;Zellweger et al., 2003) or thermal uplift of

15 polluted air from the surrounding valleys on fair weather days (Baltensperger et al., 1997;

16 Henne et al., 2005;Zellweger et al., 2000). Because of the high elevation, the accessibility and

17 the good infrastructure, the JFJ is an ideal location for in-situ measurements of atmospheric

18 background air from continental Europe (Baltensperger et al., 1997;Henne et al.,

19 2010;Zellweger et al., 2003). JFJ is also one of the currently 29 core sites of the WMO GAW

20 (Global Atmospheric Watch) programme.

2.2   In-situ NDIR measurements at Jungfraujoch

22 The KUP CO_2 measurements are based on a combined system to monitor CO_2 and O_2

23 changes in the atmosphere. The ambient air is entering through a strongly ventilated (600

24 $m^3 h^{-1}$) common inlet on the observatory's roof to a manifold, which serves many trace gas

25 analyzers, where an aliquot of it is drawn to the KUP system. The air is cryogenically dried to

26 a dew point of -90 °C (FC-100D21, FTS systems, USA). Temperature as well as pressure is

27 stabilized to avoid influences caused by ambient air density fluctuations. This allows the

28 determination of CO_2 by a NDIR spectrometer (Maihak S710) measuring at a wavelength of

29 4.26 μm with a frequency of 1 Hz and O_2 by a paramagnetic cell under highly controlled

30 conditions. Measurements are done in a cyclic sequence of 18 hours with each gas measured

for 6 minutes with only the last 115 seconds of a six minute period used for mole fraction determination, to allow for signal stabilization after changing the sample source. At the beginning of each 18-hour sequence, the system is calibrated with two reference gases (high and low span). A working gas is measured between two ambient air measurements to correct for short term variations. All measurements ending in a particular hour are used for the calculation of hourly mean CO_2 observations, which in our case includes therefore 6 ambient observation values per hour. Cylinder measurements with a known mole fraction showed a long-term precision for hourly averages better than 0.04 ppm. The accuracy of our target cylinder corresponds to less than 0.1 ppm (WMO target value for CO_2 measurements) calculated as standard deviation of the mean considering the number of independent calibration set (high span, low span, working gas).The CO_2 values are reported on the WMO X2007 scale. A multi-annual intercomparison between the NDIR system and a cavity ring-down spectroscope at JFJ showed a very good agreement of the CO_2 measurements (Schibig et al., 2015).

2.3   Column FTIR measurements at Jungfraujoch

The University of Liège has been recording atmospheric solar spectra at JFJ since the early 1950s. The current FTIR instrument is a commercially available Bruker IFS-120 HR with a resolution of up to 0.001 cm^{-1} (Mahieu et al., 1997). It features interchangeable detectors, a KBr beam-splitter and dedicated optical filters, which altogether give the possibility to cover the 1 to 14 μm spectral range (Zander et al., 2008). Here gases such as CO_2, CH_4 and H_2O show numerous absorption lines documenting contributions to the greenhouse effect. These spectra also contain information about the abundance of many additional absorbing gas species in the path between the instrument and the sun, essentially present either in the troposphere or in the stratosphere. The CO_2 data set used here has been derived from the reference total column time series produced within the framework of the NDACC monitoring program (Network for the Detection of Atmospheric Composition Change; see http://www.ndacc.org), presented previously in e.g. Zander et al. (2008; see Figure 6). In the meantime, the data set has been consistently updated, still using the SFIT-1 algorithm (version 1.09c) and a single microwindow spanning the 2024.3 – 2024.7 cm^{-1} spectral interval, whose main spectral line at 2024.564 cm^{-1} is coming from $^{13}CO_2$. The uncertainty range on the strength of this CO_2 line is estimated at 2 to less than 5 % in the HITRAN compilation (Rothman et al., 2005), leading to a systematic error on the retrieved total column

of the same magnitude. The single CO_2 a priori vertical distribution used in all retrievals is characterized by a constant mixing ratio of 338 ppm from the surface up to the tropopause, then slightly decreasing to stabilize at 330 ppm at 20 km and above. During the retrieval process, a simple scaling of the whole vertical profile is performed, accounting for interferences by weak ozone and water vapor lines, and the mixing ratio derived for CO_2 in the troposphere is used in the present comparisons. Note that the representativeness of this unique profile is not optimal for all seasons and may lead to an underestimation of the seasonal amplitude (see Fig. 1 in Barthlott et al., 2015), because of a non-optimum vertical sensitivity of the FTIR retrieval. Indeed, typical values of the total column averaging kernel – indicative of the fraction of information coming from retrieval rather than from the a priori (e.g. Vigouroux et al., 2015) – are in the $0.5 - 1$ range between the ground and 10 km altitude, in line with Fig. 4 of Barthlott et al. (2015). Over all the standard deviation of multiple measurements over the course of a single day corresponds to less than one ppm, which is significantly smaller than the observed seasonal cycle.

2.4   Data processing

The NDIR data set is much more influenced by near ground processes like thermal uplift of PBL air from the surrounding valleys, advection of PBL air by synoptic events etc. than the FTIR and shows therefore a higher variability. Additionally, because of the large volume of the column sampled by the FTIR above JFJ the CO_2 mole fraction measured by the FTIR is averaged and the data set is far less sensitive to local events than the in-situ NDIR measurements. The FTIR needs a cloudless sky to be able to measure, whereas the NDIR system is measuring under all conditions, which can lead to very high CO_2 mole fractions during e.g. Föhn events, when the sky is cloudy and polluted air from the heavily industrialized Po basin (Northern Italy) is advected to JFJ. Therefore, only measurements of background air should be taken into account to compare the two data sets properly.

2.4.1   Filtering, trend and seasonality calculation

The background data were selected using a statistical approach. A cubic spline was fitted to both datasets individually, the standard deviation of the residuals was calculated and all points beyond 2.7 σ were flagged as outliers. This process was repeated in both data sets until convergence. The threshold of 2.7 σ was chosen because in normally distributed data more

than 99 % of the total data points would be included for further calculations and only the most obvious outliers (less than 1 %) would be rejected.

The CO_2 mole fraction is dominated by two major processes. One is the linear increase due to fossil fuel combustion (trend) and one is the annual in- and decrease due to respiration and photosynthesis, and to a lesser degree due to fossil fuel combustion (seasonality). The trend was calculated for both datasets individually with a Monte Carlo approach.

For the trend calculation we intentionally used the datasets including seasonal signals because it leads to realistic trend error estimates compared to deseasonalized datasets, which in our view tend to underestimate the error. The datasets were split in two subsets, where each of the subsets spanned over n - 0.5 phases (in this study n equals 9 years) to prevent a bias in the trend calculation due to the seasonal cycle. The first subsets start in January 2005, the second subsets start in July 2005. In each subset about 2 % (a higher number does improve the result) of the points were selected randomly and the linear trend was calculated. This was repeated 500 times with each subset and the averages of these linear trends were taken as the slopes of the datasets.

To calculate the seasonality, the two datasets were detrended and monthly averages were formed, from which the seasonality was calculated as the difference between the highest and the lowest value.

2.4.2 Correlation analysis

Because of the different time resolutions for in-situ and FTIR measurements we selected those in-situ measurements (six minute and hourly NDIR averages) that are closest ($\pm$ 30 min) to the FTIR values for correlation analysis.

Since the differences between both correlation analyses were negligible (see results section), it was decided to continue with the hourly averages of the NDIR dataset only, which is the common output of the NDIR database.

The FTIR's sample volume is much bigger than the NDIR system's and because of transportation processes there's a possibility of mixing processes. To check, a moving average of the NDIR data with increasing width was calculated to see if the correlation is enhanced with expanding width (from 0 to $\pm$ 600 h).

Furthermore, the column measurements were retrieved for the layer between 3.58 km (altitude of the Sphinx Observatory) to the top atmosphere (set to 100 km in the retrieval scheme) whereas the NDIR system is measuring at the lower boundary of the FTIR's sampling

column, therefore it is possible that a time shift in the measured CO_2 mole fractions due to advection, uplift of air parcels etc. occurs. To check whether a systematic time shift exists between the two datasets, the NDIR measurements were shifted relative to the FTIR data from -60 to +60 days (corresponding to -1440 h to +1440 h) in hourly steps and again the correlation of the two data sets was calculated. If there is a systematic time shift, the deviation should be indicated by increased correlation values.

2.5   FLEXPART model runs

From 2009 to 2011, backward Lagrangian particle dispersion model simulations were performed with FLEXPART (Stohl, et al. 2005) to simulate the transport towards JFJ and estimate surface source sensitivities (footprints) of the sampled air masses. To account for the complex flow in the Alpine area, a regional scale version of the model driven by operational output from the regional scale numerical weather prediction model COSMO as produced by MeteoSwiss was used (Henne et al., 2015, Oney et al., 2015) . Since COSMO is a limited area model, the transport of particles leaving the domain was further simulated in the global scale version of FLEXPART (Stohl et al., 2005) driven by operational analysis fields of the European Centre for Medium Range Weather Forecast (ECMWF). In the Alpine area, COSMO input data had a horizontal resolution of approximately 2 km x 2 km, in Western Europe 7 km x 7 km. Of the 1214 FTIR measurements in this period, footprints were available for 766. The model simulated footprints of the surface in-situ observations and five partial columns above JFJ reaching from 3365-4226 m a.s.l., 4226-4912 m a.s.l., 4912-5629 m a.s.l., 5629-6386 m a.s.l. and 6386-7184 m a.s.l. The lower boundary is below JFJ in order to account for smoothed model topography. Particles released at and above JFJ were followed 10 days backward in time to calculate source sensitivities, represented by total residence time, which were calculated as total residence times derived by summing residence times over all start times and over all integration time steps within a selected integration interval for all grid cells as given in Henne et al. (2010). Source sensitivities were evaluated on regular longitude/latitude grids. The resolution was 0.5° x 0.5° globally, 0.2° x 0.2° over Europe and an even higher resolution of 0.1° x 0.1° was used in the Alpine area. The footprints of the individual measurements of each partial column were averaged to monthly means to get information about the origin of the air masses in the according month (Henne, 2014;Henne et al., 2013).

3 Results

Because of the different measurement techniques, the number of data points in the two datasets is different. In the period 2005 to 2013 the NDIR dataset contains 68477 hourly averages from which about 5 % were omitted as pollution or depletion events resulting from PBL influence as estimated by the filtering (Figure 1). In the same period, the FTIR dataset shows 3068 measurements of which about 5 % were rejected as pollution and depletion events, too (Figure 2). For all further calculations, only the filtered datasets were used.

The average of the detrended and deseasonalized NDIR data before and after filtering was 0.00 ± 2.65 ppm and 0.00 ± 1.84 ppm (Figure 3 A), the average of the FTIR data was 0.01 ± 2.61 ppm and 0.01 ± 2.16 ppm, respectively (Figure 3 B).

With a Monte Carlo algorithm, the values of the annual change of the CO_2 mole fraction of the two datasets were calculated. Despite the shift between the two datasets of roughly 13 ppm and the different measurement techniques the annual CO_2 increase is quite similar. The FTIR slope is 2.04 ± 0.07 ppm yr^{-1} and the NDIR dataset shows a slope of 1.97 ± 0.05 ppm yr^{-1}, so they are equal within their uncertainties (Figure 4). The observed offset between the FTIR (NDACC) and in-situ records at Jungfraujoch contrasts the comparison of NDACC and TCCON records as determined at Ny-Ålesund which do not show any offset at all when using several individual CO_2 lines for the mid-IR (Buschmann et al., 2016). However, the FTIR/NDIR offset of about 3% is commensurate with the systematic uncertainty affecting the FTIR measurement; see section 2.3.

By detrending the datasets with the derived slopes, the seasonality can be calculated. The column dataset shows a seasonality of 4.46 ± 1.11 ppm whereas the in-situ measurements at the Sphinx Observatory show a seasonality roughly twice as big, namely 10.10 ± 0.73 ppm. To find the moment of the average minima and maxima, a two harmonic fit function was applied to the detrended datasets. The minima of the FTIR and NDIR datasets are both in the middle of August, but the maxima are roughly ten weeks apart. The maximum of the NDIR datasets occurs at the end of March, whereas seasonality of the FTIR dataset already reaches its maximum in the middle of January (Figure 5).

The footprints of August, January and March, when the extrema of the seasonal cycle occurred, as calculated with FLEXPART show that the in-situ observation at Jungfraujoch is mainly receiving air masses that are influenced by Central Europe, and to a lesser degree by the Mediterranean area and the northern Atlantic (Figure 6, Figure 7 and Figure 8).

1 With increasing altitude, the footprints of the sub-columns indicate, that the measured air

2 masses become more sensitive to regions as far west as e.g. the Caribbean and the United

3 States and that the influence from the European continent and northern regions higher than

4 50°N is decreasing (Figure 6, Figure 7 and Figure 8).

5 In general, the decoupling between the FTIR columns and possible surface fluxes of CO_2

6 from land surfaces north of 30°N was strongest during the winter month (January to March),

7 when especially low surface residence times were simulated by FLEXPART for the free

8 tropospheric FTIR columns (Figure 9). From April to September larger surface residence

9 times were seen also for the FTIR columns and a stronger coupling between surface fluxes

10 and the free troposphere can be expected. At the same time residence times over tropical land

11 surface (south of 30°N) were generally larger for the FTIR columns compared to the surface

12 and were especially increased from February to April (see Figure 9).

13 To estimate the relationship between the FTIR and NDIR measurements the correlation was

14 calculated. The FTIR measurements take normally about 10 min and are done whenever

15 possible. Therefore the FTIR data is reported exactly at the measuring time. The NDIR on the

16 other hand is measuring non-stop, but only 115 s of six-minute intervals (see methods) are

17 used to calculate a data point and the six-minute data is normally averaged to hourly averages.

18 Therefore we first checked whether the high resolution data are necessary or hourly data is

19 good enough. To do so, to each FTIR data point the nearest high resolution and hourly

20 averaged NDIR values were assigned. An additional condition was that the NDIR value must

21 not be further apart than ± 30 min, otherwise no NDIR data point was set, which was the case

22 in about 10 % of the FTIR data points. The correlation between the FTIR and the high

23 resolution NDIR CO_2 measurements and between the FTIR and the hourly averages were

24 calculated to be 0.819 and 0.820, so the differences between the two regression values are

25 negligible. To examine the relationship between the FTIR and the NDIR measurements

26 further, the seasonality of the two datasets was eliminated which gave almost the same

27 correlation of 0.824 (0.838 with the high resolution data). In the next step only the trend was

28 subtracted and the remaining seasonalities were compared, which lead to a much smaller

29 correlation of 0.460 (0.461 with the high resolution data). In a final step, the trend as well as

30 the seasonality was removed, which resulted in a correlation of 0.071 (0.084 high resolution

31 data vs. FTIR). Since correlations between the FTIR data and the NDIR's high resolution and

32 the hourly data were almost the same, only the hourly data was considered for further

33 calculations (Figure 10).

1 As mentioned above, the column measurements represent the whole vertical distribution

2 above Jungfraujoch whereas the NDIR system is measuring at the base of the FTIR's

3 sampling column. Therefore, the two records might be time-delayed due to advection, uplift

4 of air parcels etc. To check for a potential time lag, the NDIR measurements were shifted

5 relative to the FTIR data from -1440 to +1440 hours in hourly steps.

6 The correlations between the NDIR and FTIR datasets and between the deseasonalized NDIR

7 and FTIR datasets show a peak region at a time shift from -10 h to 60 h with the highest

8 correlation being 0.830 and 0.836 respectively (Figure 11 A, Figure 11 B). The correlation

9 between the datasets is decreasing before and after this range, in the deseasonalized datasets

10 the correlation stays more or less stable. The correlation between the two trend corrected

11 datasets shows a plateau of enhanced correlation values from -50 h to 200 h time shift with a

12 maximum correlation of 0.495 at a time shift of 165 h, at lower and higher time shifts, the

13 correlation is decreasing (Figure 11 C). The correlation of the detrended and deseasonalized

14 datasets shows no distinct pattern and is oscillating around 0 (Figure 11 D).

15 Since the air volume measured by the FTIR is much bigger than the NDIR system's volume,

16 vertical mixing and transport processes can occur and thereby changing the CO_2 mole fraction

17 in the measured air parcels. Therefore moving averages with increasing widths (up to $\pm$ 600 h)

18 were calculated from the NDIR data and the obtained averaged NDIR values were correlated

19 with the filtered FTIR dataset. Changing the width of the moving average doesn't have a

20 strong influence on the correlation between the two filtered datasets, because the increasing

21 width of the moving average just smooths the dataset. The correlation remains at about 0.85

22 (Figure 12 A), with a very small increase of the correlation at the beginning, most probably

23 due to the above mentioned smoothing effect. The same is true for the correlation between the

24 deseasonalized datasets. They show high correlation of about 0.84 over the whole range of

25 widths, with a slight increase at the beginning, which is not significant (Figure 12 B). By

26 detrending the datasets, the correlation is increasing with the width of the moving average and

27 shows a plateau of higher correlation of about 0.5 at a width 150 to 600 h from where on it is

28 decreasing again (Figure 12 C). However, the changes in the correlation within the range of

29 150 h to 600 h are very small. The detrended and deseasonalized datasets show a very low

30 correlation and the improvement of the correlation due to the changing width of the moving

31 average is negligible. Over all, the improvement of the correlations due to the changing width

32 of the moving average is very small (Figure 12 D).

1   Finally both, the time shift and the width of the moving average were varied about ± 1440 h

2   and ± 600 h, to see with which combination of time shift and width the best correlation can be

3   reached. They all show a ridge of higher correlation at a time shift around zero which is

4   broadening with increasing width of the moving average, except for the data without slope

5   and seasonality, which have a low correlation anyway (Figure 13). The increasing width of

6   the moving average leads to a small improvement of the correlations in the beginning,

7   however over all it doesn't seem to have a strong influence on the correlations. The time shift

8   on the other hand has an influence on correlation between the complete filtered datasets and

9   even more on the correlation of the detrended datasets. In the correlation of the

10   deseasonalized datasets, the influence of the time shift is very limited except for the small

11   ridge of slightly enhanced correlations around zero time shift as mentioned above.

4   Discussion

14   The filtered FTIR and NDIR datasets show a very similar increase in the CO_2 mole fraction of

15   ambient air, despite the two totally different measurement principles. The calculated annual

16   CO_2 trends of the FTIR and NDIR datasets are 2.04 ± 0.07 ppm yr^{-1} and 1.97 ± 0.05 ppm yr^{-1}

17   respectively (Figure 4) and are in good agreement with flask measurements done at JFJ with a

18   slope of 1.85 ppm yr^{-1} (van der Laan-Luijkx et al., 2013) and other remote stations in the

19   northern hemisphere; for example Mauna Loa with 2.05 ppm yr^{-1} (Tans and Keeling, 2014) or

20   Alert with 1.85 ppm yr^{-1} (Keeling et al., 2001). Also the NDIR dataset's average seasonality

21   of 10.10 ± 0.73 ppm is in good agreement with the seasonality of these flask measurements,

22   which were 10.54 ± 0.18 ppm in the period 2007 to 2011 (van der Laan-Luijkx et al., 2013)

23   and is roughly double the FTIR's average seasonality of 4.46 ± 1.11 ppm (Figure 5). The

24   lower seasonality of the FTIR dataset can be explained by the fact that the NDIR system is

25   measuring CO_2 mole fractions at the Sphinx Observatory, which is most of the time above the

26   PBL (Henne et al., 2010) but still closer to the ground than the FTIR measurements.

27   Therefore the signal of the biosphere is stronger than in the column, where it is attenuated by

28   vertical mixing and transport processes of the atmosphere with increasing height. Also the

29   fixed a priori vertical CO_2 profile may contribute partly to the lower seasonality of the FTIR

30   measurements. The shape of the profile used to retrieve the CO_2 data doesn't reproduce the

31   changes due to seasonality and is therefore not always the optimum. By using a seasonally

32   varying a priori retrieval the seasonality might be slightly higher because the amplitude of

1   CO_2 is better retrieved (Barthlott et al., 2015). Furthermore, in the tropopause and the lower

2   stratosphere, the phase of the CO_2 seasonality is shifted by several months (Bönisch et al.,

3   2008;Gurk et al., 2008;Bönisch et al., 2009). However, this has only a minor influence on the

4   observed dampening of the amplitude of the FTIR seasonality compared to the vertical

5   mixing, since the stratosphere contains only about 10 % of the abundance of atmospheric air

6   molecules.

7   It is not easy to define the seasonal minimum and maximum in the FTIR dataset because they

8   are not very clearly pronounced. By fitting a two harmonic function the minimum was found

9   to be in the middle of August, the maximum in the middle of January. While the minimum of

10   the NDIR dataset is around the same time, the maximum of the FTIR dataset occurs roughly

11   ten weeks earlier than the maxima of the NDIR dataset (Figure 5). The timing of the minima

12   of both datasets and the maximum of the NDIR dataset coincide quite well with net land-

13   atmosphere carbon flux changes from negative to positive values and vice versa (Zeng et al.,

14   2014). Therefore an alternative explanation is needed for the early maximum of the FTIR

15   dataset. Sensitivity analyses revealed that the upper tropospheric air originates from different

16   geographic regions, mainly from south west, than the in-situ air measured by the NDIR.

17   During summer, the NDIR measurements record mainly air from European regions, whereas

18   the FTIR sees more influence from the west (Figure 6). From winter to spring, NDIR CO_2

19   values are again driven by European sources, whereas FTIR values represent a significantly

20   wider foot print reaching to west and further to the north in contrast to the summer situation

21   (Figure 7, Figure 8). Similar studies investigating CO at JFJ also showed that JFJ is not only

22   sensitive to Central Europe but also to regions as far west as for example North America, the

23   Pacific or even Asia and that the influence of these regions is getting stronger with increasing

24   height (Dils et al., 2011;Pfister et al., 2004;Zellweger et al., 2009). Therefore the air measured

25   by the FTIR is partially decoupled from the increasing CO_2 values of the winter-time northern

26   hemisphere. Furthermore, the decoupling might be amplified by the weak overturn of

27   tropospheric air in winter. Towards spring, the tropospheric overturn speeds up again which

28   results in synchronous CO_2 minima for both datasets in August (Figure 9).These findings can

29   help to understand the shift in the observed wintertime maximum of CO_2 between FTIR

30   (January) and NDIR (March-April). The land surfaces of northern hemispheric midlatitudes

31   act as a net CO_2 source during the winter half year, since photosynthesis is largely reduced

32   and respiration and anthropogenic emissions of CO_2 dominate the budget. Hence, the

33   maximum of CO_2 is observed at the end of the winter half year and close to the surface. For

the free troposphere above JFJ as observed by the FTIR the direct link to these wintertime releases of CO_2 is weakened due to generally reduced vertical transport. At the same time more frequent transport from and land surface contact in the tropics can be deduced (Figure 9), an area that even during the winter half year may act as a net CO_2 sink due to photosynthetic uptake. An earlier onset of decreasing CO_2 in the free troposphere above JFJ could thereby be explained by different seasonality of transport and vertical mixing. Additionally, the assumption of a fixed a priori CO_2 vertical distribution to retrieve the column integrated CO_2 concentration from the FTIR dataset may contribute partially to the observed shift of ten weeks in the NDIR and FTIR maxima, because it is representing the distribution in winter/spring inadequately.

Another hint that the two systems are not measuring the same air parcels can be found in correlation analyses. After omitting outliers, which are mostly caused by synoptic events, thermal uplift of polluted air from surrounding valleys, or other local to regional transport events, the correlation of the two datasets is as large as 0.820, which is quite encouraging considering the different nature of the measurements. By excluding the seasonality from both datasets, the correlation stays almost the same, namely 0.824 but drops to 0.460 if the seasonality is included but the annual CO_2 increase is subtracted. The comparison of the two CO_2 datasets with the annual CO_2 increase and the seasonality subtracted showed a very low correlation of 0.071, which is negligible (Figure 10). Because of possible delays and mixing effects of the CO_2 signal, the time shift as well as the width of the moving average calculated on the hourly values of the NDIR CO_2 values was varied between $\pm$ 1440 h and up to $\pm$ 600 h, respectively. Shifting the NDIR time relative to the FTIR measurement time creates a ridge of higher correlations around 0 h time shift with a slight tendency towards positive values (Figure 13 A). This ridge-like form is clearly pronounced in the correlation plot between the complete filtered FTIR and NDIR datasets and even more in the datasets without slope (Figure 13 C) than in the correlation of the datasets without seasonality (Figure 13 B). There it is very small and the correlation is high across the whole time shift and averaging width. The constantly high correlation for deseasonalized datasets is due to both datasets containing mostly background air whose CO_2 mole fraction changes are mainly driven by the annual CO_2 increase and by the seasonality of the CO_2 signal. Since the larger of the two, the seasonality, is subtracted the high correlation is mainly driven by the slope which was calculated to be the same within uncertainties and stays more or less constant over the examined period. Therefore, the time shift has almost no influence. The remaining fluctuations in the CO_2 mole

fractions with higher frequencies than the seasonality seem to play a minor role, because they're almost not visible in the comparison of the datasets without seasonality except for the small ridge (Figure 13 B), or there's no correlation at all, as in the comparison of the two datasets without slope and seasonality (Figure 13 D). This is indicating that the two measurement systems are not measuring the same air parcels, even not with a certain delay, or that the CO_2 signal of the NDIR system which is measured at the lower end of the FTIR column becomes diluted beyond recognition for FTIR by the air mixing processes. The positive effect of the increasing width of the moving average on the correlation is strongest, but still very low, around the first 100 h. Afterwards its main effect is broadening the ridge of the slightly enhanced correlations. The reason for the broadening effect of the increasing width is its smoothing effect on the NDIR values. With increasing width, the influence of a specific NDIR point on the correlation becomes smaller and the NDIR dataset evolves into a smooth sine like curve with decreasing amplitudes, similar to the FTIR dataset, where this form is caused by the higher sampling volume and the dampening due to mixing processes in the atmosphere. However, the small influence of the moving average's width on the correlation means that the correlation of the in-situ and the column measurement is mainly influenced by the slope and the seasonality. Short term fluctuations play a minor role mainly because either their CO_2 signal is dampened too much to be seen in the column measurement or it is not measured at all as e.g. diurnal cycles because of the applied measurement methods.

5 Conclusions

Two datasets of CO_2 measurements at the High Altitude Research Station Jungfraujoch in the period 2005 to 2013 were compared. The FTIR system is measuring the attenuation of solar light at different wavelengths caused by molecules of light absorbing gas species in the column between the Sphinx Observatory and the sun. From the obtained spectra, with the knowledge of CO_2 specific extinction bands and the pressure distribution along the path of the light, it is possible to calculate the CO_2 mole fraction in the column. The NDIR system is measuring the CO_2 mole fraction of ambient air at the Sphinx Observatory which corresponds to the lower boundary of the FTIR measurements. The two datasets were filtered with a statistical approach to exclude CO_2 measurements which were influenced by recent transport from the planetary boundary layer. The filtering caused a loss of about 5 % in both, the NDIR and the FTIR dataset.

The annual CO_2 increase of the two datasets was calculated with a Monte Carlo approach. Despite an average offset of 13 ppm between the two datasets, which is within the systematic uncertainty affecting the FTIR measurement, the slopes were in good agreement, namely 2.04 $\pm$ 0.07 ppm yr^{-1} in the FTIR measurements and 1.97 $\pm$ 0.05 ppm yr^{-1} in the NDIR dataset. The seasonality of the CO_2 signal of the NDIR and the FTIR system is 10.10 $\pm$ 0.73 ppm and 4.46 $\pm$ 1.11 ppm, respectively. The difference is caused by a dampening of the CO_2 signal with increasing altitude due to mixing processes. While the minima of the two datasets both occur in the simultaneously, the maxima of the FTIR dataset was found ten weeks earlier than the NDIR maxima.

The difference in the occurrence of the minima is most probably caused by the different transport history of the air masses measured at JFJ and in the column above JFJ. In January, the in-situ system is measuring air from central Europe and the Mediterranean, whereas the air masses of the column measurements are more affected by the subtropic Northern Atlantic. With the onset of spring in Europe, the photosynthetic activity is increasing and the CO_2 mole fraction of air measured by the in-situ system starts to decrease at the end of March. The two filtered datasets as well as the two deseasonalized datasets show a high correlation, whereas the correlation between the two detrended datasets is only mediocre and inexistent in the between the two detrended and deseasonalized datasets. Neither shifting the time of the NDIR measurements relative to the FTIR measurements nor increasing the width of the moving average did increase the correlation between the two datasets significantly. The enhanced correlation values around a time shift of zero indicates that (i) there isn't a systematic time shift apparent and that (ii) the correlation between the two datasets is mainly driven by the annual CO_2 increase and to a lesser degree by the seasonality. Therefore both measurement systems are suitable to measure the annual CO_2 increase, because this signal is well mixed within the atmosphere. Short term variations as the seasonality or daily variations are less or not comparable, because (a) the transport history of the air parcels measured is different, (b) the signal is mixed beyond recognition or (c) since the FTIR has a low vertical sensitivity it was not exploited in the present retrievals and therefore the measured column signal contains mixed information from the troposphere and the stratosphere.

Acknowledgements

This work was financially supported by the Swiss National Science Foundation (SNF-Project 200020_134641) and the Federal Office of Meteorology and Climatology MeteoSwiss in the

1   framework of Swiss GCOS. We like to thank the International Foundation High Altitude

2   Research Stations Jungfraujoch and Gornergrat (HFSJG), especially the custodians Martin

3   Fischer, Felix Seiler and Urs Otz for changing the calibration gases cylinders of the NDIR

4   system and other maintenance work. Additionally the authors like to thank Hanspeter Moret

5   and Peter Nyfeler for his precious work and help in maintaining and repairing the systems in

6   the Laboratory in Bern and also at Jungfraujoch. The Belgian contribution to the present work

7   was mainly supported by the Belgian Science Policy Office (BELSPO) and the Fonds de la

8   Recherche Scientifique – FNRS, both in Brussels. FLEXPART simulations were carried out

9   in the framework of EC FP7 project NORS (grant agreement N° 284421). Additional support

10   was provided by MeteoSwiss (GAW-CH) and the Fédération Wallonie Bruxelles. We are

11   grateful to the many colleagues and collaborators who have contributed to FTIR data

12   acquisition.

References

Arrhenius, S.: XXXI. On the influence of carbonic acid in the air upon the temperature of the ground, Philosophical Magazine Series 5, 41, 237-276, 10.1080/14786449608620846, 1896.

Baltensperger, U., Gäggeler, H. W., Jost, D. T., Lugauer, M., Schwikowski, M., Weingartner, E., and Seibert, P.: Aerosol climatology at the high-alpine site Jungfraujoch, Switzerland, Journal of Geophysical Research: Atmospheres, 102, 19707-19715, 10.1029/97JD00928, 1997.

Barthlott, S., Schneider, M., Hase, F., Wiegele, A., Christner, E., González, Y., Blumenstock, T., Dohe, S., García, O. E., Sepúlveda, E., Strong, K., Mendonca, J., Weaver, D., Palm, M., Deutscher, N. M., Warneke, T., Notholt, J., Lejeune, B., Mahieu, E., Jones, N., Griffith, D. W. T., Velazco, V. A., Smale, D., Robinson, J., Kivi, R., Heikkinen, P. and Raffalski, U.: Using XCO2 retrievals for assessing the long-term consistency of NDACC/FTIR data sets, Atmospheric Measurement Techniques, 8(3), 1555–1573, doi:10.5194/amt-8-1555-2015, 2015.

Bender, M. L., Ho, D. T., Hendricks, M. B., Mika, R., Battle, M. O., Tans, P. P., Conway, T. J., Sturtevant, B., and Cassar, N.: Atmospheric O_2/N_2 changes, 1993–2002: Implications for the partitioning of fossil fuel CO_2 sequestration, Global Biogeochemical Cycles, 19, GB4017, 10.1029/2004GB002410, 2005.

Bönisch, H., Hoor, P., Gurk, C., Feng, W., Chipperfield, M., Engel, A., and Bregman, B.: Model evaluation of CO_2 and SF_6 in the extratropical UT/LS region, Journal of Geophysical Research: Atmospheres, 113, 10.1029/2007JD008829, 2008.

Bönisch, H., Engel, A., Curtius, J., Birner, T., and Hoor, P.: Quantifying transport into the lowermost stratosphere using simultaneous in-situ measurements of SF_6 and CO_2, Atmos. Chem. Phys., 9, 5905-5919, 10.5194/acp-9-5905-2009, 2009.

Bousquet, P., Gaudry, A., Ciais, P., Kazan, V., Monfray, P., Simmonds, P. G., Jennings, S. G., and O'Connor, T. C.: Atmospheric CO_2 concentration variations recorded at Mace Head, Ireland, from 1992 to 1994, Physics and Chemistry of the Earth, 21, 477-481, http://dx.doi.org/10.1016/S0079-1946(97)81145-7, 1996.

Brenninkmeijer, C. A. M., Crutzen, P., Boumard, F., Dauer, T., Dix, B., Ebinghaus, R., Filippi, D., Fischer, H., Franke, H., Frieβ, U., Heintzenberg, J., Helleis, F., Hermann, M.,

Kock, H. H., Koeppel, C., Lelieveld, J., Leuenberger, M., Martinsson, B. G., Miemczyk, S., Moret, H. P., Nguyen, H. N., Nyfeler, P., Oram, D., O'Sullivan, D., Penkett, S., Platt, U., Pupek, M., Ramonet, M., Randa, B., Reichelt, M., Rhee, T. S., Rohwer, J., Rosenfeld, K., Scharffe, D., Schlager, H., Schumann, U., Slemr, F., Sprung, D., Stock, P., Thaler, R., Valentino, F., van Velthoven, P., Waibel, A., Wandel, A., Waschitschek, K., Wiedensohler, A., Xueref-Remy, I., Zahn, A., Zech, U., and Ziereis, H.: Civil Aircraft for the regular investigation of the atmosphere based on an instrumented container: The new CARIBIC system, Atmos. Chem. Phys., 7, 4953-4976, 10.5194/acp-7-4953-2007, 2007.

Broecker, W. S., and Peng, T.-H.: Tracers in the Sea, Lamont-Doherty Geological Observatory, Palisades, New York, 1982.

Buchwitz, M., de Beek, R., Noël, S., Burrows, J. P., Bovensmann, H., Schneising, O., Khlystova, I., Bruns, M., Bremer, H., Bergamaschi, P., Körner, S., and Heimann, M.: Atmospheric carbon gases retrieved from SCIAMACHY by WFM-DOAS: version 0.5 CO and CH_4 and impact of calibration improvements on CO_2 retrieval, Atmos. Chem. Phys., 6, 2727-2751, 10.5194/acp-6-2727-2006, 2006.

Buschmann, M., Deutscher, N. M., Sherlock, V., Palm, M., Warneke, T., and Notholt, J.: Retrieval of xCO_2 from ground-based mid-infrared (NDACC) solar absorption spectra and comparison to TCCON, Atmos. Meas. Tech., 9, 577-585, 10.5194/amt-9-577-2016, 2016.

Butz, A., Guerlet, S., Hasekamp, O., Schepers, D., Galli, A., Aben, I., Frankenberg, C., Hartmann, J. M., Tran, H., Kuze, A., Keppel-Aleks, G., Toon, G., Wunch, D., Wennberg, P., Deutscher, N., Griffith, D., Macatangay, R., Messerschmidt, J., Notholt, J., and Warneke, T.: Toward accurate CO_2 and CH_4 observations from GOSAT, Geophysical Research Letters, 38, 10.1029/2011GL047888, 2011.

Crisp, D., Atlas, R. M., Breon, F. M., Brown, L. R., Burrows, J. P., Ciais, P., Connor, B. J., Doney, S. C., Fung, I. Y., Jacob, D. J., Miller, C. E., O'Brien, D., Pawson, S., Randerson, J. T., Rayner, P., Salawitch, R. J., Sander, S. P., Sen, B., Stephens, G. L., Tans, P. P., Toon, G. C., Wennberg, P. O., Wofsy, S. C., Yung, Y. L., Kuang, Z., Chudasama, B., Sprague, G., Weiss, B., Pollock, R., Kenyon, D., and Schroll, S.: The Orbiting Carbon Observatory (OCO) mission, Advances in Space Research, 34, 700-709, http://dx.doi.org/10.1016/j.asr.2003.08.062, 2004.

1 Chevallier, F., Maksyutov, S., Bousquet, P., Bréon, F.-M., Saito, R., Yoshida, Y., and Yokota,

2 T.: On the accuracy of the CO_2 surface fluxes to be estimated from the GOSAT observations,

3 Geophysical Research Letters, 36, n/a-n/a, 10.1029/2009GL040108, 2009.

4 Chevallier, F., Ciais, P., Conway, T. J., Aalto, T., Anderson, B. E., Bousquet, P., Brunke, E.

5 G., Ciattaglia, L., Esaki, Y., Fröhlich, M., Gomez, A., Gomez-Pelaez, A. J., Haszpra, L.,

6 Krummel, P. B., Langenfelds, R. L., Leuenberger, M., Machida, T., Maignan, F., Matsueda,

7 H., Morguí, J. A., Mukai, H., Nakazawa, T., Peylin, P., Ramonet, M., Rivier, L., Sawa, Y.,

8 Schmidt, M., Steele, L. P., Vay, S. A., Vermeulen, A. T., Wofsy, S., and Worthy, D.: CO_2

9 surface fluxes at grid point scale estimated from a global 21 year reanalysis of atmospheric

10 measurements, Journal of Geophysical Research: Atmospheres, 115, D21307,

11 10.1029/2010JD013887, 2010.

12 Dils, B., De Mazière, M., Müller, J. F., Blumenstock, T., Buchwitz, M., de Beek, R.,

13 Demoulin, P., Duchatelet, P., Fast, H., Frankenberg, C., Gloudemans, A., Griffith, D., Jones,

14 N., Kerzenmacher, T., Kramer, I., Mahieu, E., Mellqvist, J., Mittermeier, R. L., Notholt, J.,

15 Rinsland, C. P., Schrijver, H., Smale, D., Strandberg, A., Straume, A. G., Stremme, W.,

16 Strong, K., Sussmann, R., Taylor, J., van den Broek, M., Velazco, V., Wagner, T., Warneke,

17 T., Wiacek, A., and Wood, S.: Comparisons between SCIAMACHY and ground-based FTIR

18 data for total columns of CO, CH_4, CO_2 and N_2O, Atmos. Chem. Phys., 6, 1953-1976,

19 10.5194/acp-6-1953-2006, 2006.

20 Dils, B., Cui, J., Henne, S., Mahieu, E., Steinbacher, M., and De Mazière, M.: 1997–2007 CO

21 trend at the high Alpine site Jungfraujoch: a comparison between NDIR surface in situ and

22 FTIR remote sensing observations, Atmos. Chem. Phys., 11, 6735-6748, 10.5194/acp-11-

23 6735-2011, 2011.

24 Feely, R. A., Sabine, C. L., Lee, K., Berelson, W., Kleypas, J., Fabry, V. J., and Millero, F. J.:

25 Impact of Anthropogenic CO_2 on the $CaCO_3$ System in the Oceans, Science, 305, 362-366,

26 10.1126/science.1097329, 2004.

27 Gurk, C., Fischer, H., Hoor, P., Lawrence, M. G., Lelieveld, J., and Wernli, H.: Airborne in-

28 situ measurements of vertical, seasonal and latitudinal distributions of carbon dioxide over

29 Europe, Atmos. Chem. Phys., 8, 6395-6403, 10.5194/acp-8-6395-2008, 2008.

30 Halloran, P. R.: Does atmospheric CO_2 seasonality play an important role in governing the

31 air-sea flux of CO_2?, Biogeosciences, 9, 2311-2323, 10.5194/bg-9-2311-2012, 2012.

Heinze, C., Maier-Reimer, E., and Winn, K.: Glacial pCO_2 Reduction by the World Ocean: Experiments With the Hamburg Carbon Cycle Model, Paleoceanography, 6, 395-430, 10.1029/91PA00489, 1991.

Henne, S., Furger, M., and Prévôt, A. S. H.: Climatology of Mountain Venting–Induced Elevated Moisture Layers in the Lee of the Alps, JOURNAL OF APPLIED METEOROLOGY, 44, 620-633, 10.1175/JAM2217.1, 2005.

Henne, S., Brunner, D., Folini, D., Solberg, S., Klausen, J., and Buchmann, B.: Assessment of parameters describing representativeness of air quality in-situ measurement sites, Atmos. Chem. Phys., 10, 3561-3581, 10.5194/acp-10-3561-2010, 2010.

Henne, S., Steinbacher, M., Mahieu, E., Bader, W., Blumenstock, T., Cuevas-Agulló, E., Brunner, D., and Buchmann, B.: Comparison of ground-based remote sensing and in-situ observations of CO, CH_4 and O_3 accounting for representativeness uncertainty, EGU General Assembly, Vienna, Austria, 7-12 April 2013, 2013.

Henne, S., D. Brunner, B. Oney, M. Leuenberger, W. Eugster, I. Bamberger, F. Meinhardt, M. Steinbacher, and L. Emmenegger, Validation of Swiss Methane Emission Inventory by Atmospheric Observations and Inverse Modelling, Atmos. Chem. Phys. Discuss., 15, 35417-35484, doi: 10.5194/acpd-15-35417-2015, 2015.

Heymann, J., Reuter, M., Hilker, M., Buchwitz, M., Schneising, O., Bovensmann, H., Burrows, J. P., Kuze, A., Suto, H., Deutscher, N. M., Dubey, M. K., Griffith, D. W. T., Hase, F., Kawakami, S., Kivi, R., Morino, I., Petri, C., Roehl, C., Schneider, M., Sherlock, V., Sussmann, R., Velazco, V. A., Warneke, T., and Wunch, D.: Consistent satellite XCO_2 retrievals from SCIAMACHY and GOSAT using the BESD algorithm, Atmos. Meas. Tech., 8, 2961-2980, 10.5194/amt-8-2961-2015, 2015.

IPCC: Climate Change 2013: The Physical Science Basis. Contribution of Working Group I to the Fifth Assessment Report of the Intergovernmental Panel on Climate Change, Cambridge University Press, Cambridge, United Kingdom and New York, NY, USA, 1535 pp., 2013.

Karl, T. R., and Trenberth, K. E.: Modern Global Climate Change, Science, 302, 1719-1723, 10.1126/science.1090228, 2003.

Keeling, C. D., Bacastow, R. B., Bainbridge, A. E., Ekdahl, C. A., Guenther, P. R., Waterman, L. S., and Chin, J. F. S.: Atmospheric carbon dioxide variations at Mauna Loa Observatory, Hawaii, Tellus, 28, 538-551, 10.1111/j.2153-3490.1976.tb00701.x, 1976.

Keeling, C. D., Whorf, T. P., Wahlen, M., and van der Plichtt, J.: Interannual extremes in the rate of rise of atmospheric carbon dioxide since 1980, Nature, 375, 666-670, 1995.

Keeling, C. D., Piper, S. C., Bacastow, R. B., Wahlen, M., Whorf, T. P., Heimann, M., and Meijer, H. A.: Exchanges of Atmospheric CO_2 and $^{13}CO_2$ with the Terrestrial Biosphere and Oceans from 1978 to 2000. I. Global Aspects, SIO Reference Series, No. 01-06, Scripps Institution of Oceanography, San Diego, 88, 2001.

Komhyr, W. D., Gammon, R. H., Harris, T. B., Waterman, L. S., Conway, T. J., Taylor, W. R., and Thoning, K. W.: GLOBAL ATMOSPHERIC CO_2 DISTRIBUTION AND VARIATIONS FROM 1968-1982 NOAA GMCC CO_2 FLASK SAMPLE DATA, J. Geophys. Res.-Atmos., 90, 5567-5596, 10.1029/JD090iD03p05567, 1985.

Le Quéré, C., Peters, G. P., Andres, R. J., Andrew, R. M., Boden, T., Ciais, P., Friedlingstein, P., Houghton, R. A., Marland, G., Moriarty, R., Sitch, S., Tans, P., Arneth, A., Arvanitis, A., Bakker, D. C. E., Bopp, L., Canadell, J. G., Chini, L. P., Doney, S. C., Harper, A., Harris, I., House, J. I., Jain, A. K., Jones, S. D., Kato, E., Keeling, R. F., Klein Goldewijk, K., Körtzinger, A., Koven, C., Lefèvre, N., Omar, A., Ono, T., Park, G. H., Pfeil, B., Poulter, B., Raupach, M. R., Regnier, P., Rödenbeck, C., Saito, S., Schwinger, J., Segschneider, J., Stocker, B. D., Tilbrook, B., van Heuven, S., Viovy, N., Wanninkhof, R., Wiltshire, A., Zaehle, S., and Yue, C.: Global carbon budget 2013, Earth Syst. Sci. Data Discuss., 6, 689-760, 10.5194/essdd-6-689-2013, 2013.

Machida, T., Kita, K., Kondo, Y., Blake, D., Kawakami, S., Inoue, G., and Ogawa, T.: Vertical and meridional distributions of the atmospheric CO_2 mixing ratio between northern midlatitudes and southern subtropics, Journal of Geophysical Research: Atmospheres, 107, 8401, 10.1029/2001JD000910, 2002.

Machida, T., Matsueda, H., Sawa, Y., Nakagawa, Y., Hirotani, K., Kondo, N., Goto, K., Nakazawa, T., Ishikawa, K., and Ogawa, T.: Worldwide Measurements of Atmospheric CO_2 and Other Trace Gas Species Using Commercial Airlines, Journal of Atmospheric and Oceanic Technology, 25, 1744-1754, 10.1175/2008JTECHA1082.1, 2008.

1   Mahieu, E., Zander, R., Delbouille, L., Demoulin, P., Roland, G., and Servais, C.: Observed
2   Trends in Total Vertical Column Abundances of Atmospheric Gases from IR Solar Spectra
3   Recorded at the Jungfraujoch, Journal of Atmospheric Chemistry, 28, 227-243,
4   10.1023/A:1005854926740, 1997.

5   Messager, C., Schmidt, M., Ramonet, M., Bousquet, P., Simmonds, P., Manning, A., Kazan,
6   V., Spain, G., Jennings, S. G., and Ciais, P.: Ten years of CO_2, CH_4, CO and N_2O fluxes over
7   Western Europe inferred from atmospheric measurements at Mace Head, Ireland, Atmos.
8   Chem. Phys. Discuss., 8, 1191-1237, 10.5194/acpd-8-1191-2008, 2008.

9   Morino, I., Uchino, O., Inoue, M., Yoshida, Y., Yokota, T., Wennberg, P. O., Toon, G. C.,
10   Wunch, D., Roehl, C. M., Notholt, J., Warneke, T., Messerschmidt, J., Griffith, D. W. T.,
11   Deutscher, N. M., Sherlock, V., Connor, B., Robinson, J., Sussmann, R., and Rettinger, M.:
12   Preliminary validation of column-averaged volume mixing ratios of carbon dioxide and
13   methane retrieved from GOSAT short-wavelength infrared spectra, Atmos. Meas. Tech., 4,
14   1061-1076, 10.5194/amt-4-1061-2011, 2011.

15   Oney, B., Henne, S., Gruber, N., Leuenberger, M., Bamberger, I., Eugster, W., and Brunner,
16   D.: The CarboCount CH sites: characterization of a dense greenhouse gas observation
17   network, Atmos. Chem. Phys. Discuss., 15, 12911-12956, 10.5194/acpd-15-12911-2015,
18   2015.

19   Pales, J. C., and Keeling, C. D.: The concentration of atmospheric carbon dioxide in Hawaii,
20   Journal of Geophysical Research, 70, 6053-6076, 10.1029/JZ070i024p06053, 1965.

21   Pfister, G., Pétron, G., Emmons, L. K., Gille, J. C., Edwards, D. P., Lamarque, J. F., Attie, J.
22   L., Granier, C., and Novelli, P. C.: Evaluation of CO simulations and the analysis of the CO
23   budget for Europe, Journal of Geophysical Research: Atmospheres, 109, D19304,
24   10.1029/2004JD004691, 2004.

25   Pollock, R., Haring, R. E., Holden, J. R., Johnson, D. L., Kapitanoff, A., Mohlman, D.,
26   Phillips, C., Randall, D., Rechsteiner, D., Rivera, J., Rodriguez, J. I., Schwochert, M. A., and
27   Sutin, B. M.: The Orbiting Carbon Observatory nstrument: performance of the OCO
28   instrument and plans for the OCO-2 instrument, 2010, 78260W-78260W-78213, 2010.

1 Revelle, R., and Suess, H. E.: Carbon Dioxide Exchange Between Atmosphere and Ocean and

2 the Question of an Increase of Atmospheric CO_2 during the Past Decades, Tellus, 9, 18-27,

3 10.1111/j.2153-3490.1957.tb01849.x, 1957.

4 Rothman, L. S., Jacquemart, D., Barbe, A., Chris Benner, D., Birk, M., Brown, L. R., Carleer,

5 M. R., Chackerian, C., Chance, K., Coudert, L. H., Dana, V., Devi, V. M., Flaud, J.-M.,

6 Gamache, R. R., Goldman, A., Hartmann, J.-M., Jucks, K. W., Maki, A. G., Mandin, J.-Y.,

7 Massie, S. T., Orphal, J., Perrin, A., Rinsland, C. P., Smith, M. A. H., Tennyson, J.,

8 Tolchenov, R. N., Toth, R. A., Vander Auwera, J., Varanasi, P. and Wagner, G.: The

9 HITRAN 2004 molecular spectroscopic database, Journal of Quantitative Spectroscopy and

10 Radiative Transfer, 96(2), 139–204, doi:10.1016/j.jqsrt.2004.10.008, 2005.

11 Sabine, C. L., Feely, R. A., Gruber, N., Key, R. M., Lee, K., Bullister, J. L., Wanninkhof, R.,

12 Wong, C. S., Wallace, D. W. R., Tilbrook, B., Millero, F. J., Peng, T.-H., Kozyr, A., Ono, T.,

13 and Rios, A. F.: The Oceanic Sink for Anthropogenic CO_2, Science, 305, 367-371,

14 10.1126/science.1097403, 2004.

15 Sillén, L. G.: Regulation of O_2, N_2 and CO_2 in the atmosphere; thoughts of a laboratory

16 chemist, Tellus, 18, 198-206, 10.1111/j.2153-3490.1966.tb00226.x, 1966.

17 Stohl, A., Forster, C., Frank, A., Seibert, P., and Wotawa, G.: Technical note: The Lagrangian

18 particle dispersion model FLEXPART version 6.2, Atmos. Chem. Phys., 5, 2461-2474,

19 10.5194/acp-5-2461-2005, 2005.

20 NOAA Earth System Research Laboratory, Global Monitoring Division:

21 http://www.esrl.noaa.gov/gmd/ccgg/trends/, access: 30.10.2014, 2014.

22 Schibig, M. F., Steinbacher, M., Buchmann, B., van der Laan-Luijkx, I. T., van der Laan, S.,

23 Ranjan, S., and Leuenberger, M. C.: Comparison of continuous in situ CO_2 observations at

24 Jungfraujoch using two different measurement techniques, Atmos. Meas. Tech., 8, 57-68,

25 10.5194/amt-8-57-2015, 2015.

26 Tans, P. P., Fung, I. Y., and Takahashi, T.: Observational Contrains on the Global

27 Atmospheric CO_2 Budget, Science, 247, 1431-1438, 10.1126/science.247.4949.1431, 1990.

28 Thompson, D. R., Chris Benner, D., Brown, L. R., Crisp, D., Malathy Devi, V., Jiang, Y.,

29 Natraj, V., Oyafuso, F., Sung, K., Wunch, D., Castaño, R., and Miller, C. E.: Atmospheric

30 validation of high accuracy CO_2 absorption coefficients for the OCO-2 mission, Journal of

Quantitative Spectroscopy and Radiative Transfer, 113, 2265-2276, http://dx.doi.org/10.1016/j.jqsrt.2012.05.021, 2012.

Thoning, K. W., Tans, P. P., and Komhyr, W. D.: Atmospheric carbon dioxide at Mauna Loa Observatory: 2. Analysis of the NOAA GMCC data, 1974–1985, Journal of Geophysical Research: Atmospheres, 94, 8549-8565, 10.1029/JD094iD06p08549, 1989.

Trolier, M., White, J. W. C., Tans, P. P., Masarie, K. A., and Gemery, P. A.: Monitoring the isotopic composition of atmospheric CO_2: Measurements from the NOAA Global Air Sampling Network, Journal of Geophysical Research: Atmospheres, 101, 25897-25916, 10.1029/96JD02363, 1996.

Uglietti, C., Leuenberger, M., and Brunner, D.: European source and sink areas of CO_2 retrieved from Lagrangian transport model interpretation of combined O_2 and CO_2 measurements at the high alpine research station Jungfraujoch, Atmos. Chem. Phys., 11, 8017-8036, 10.5194/acp-11-8017-2011, 2011.

van der Laan-Luijkx, I. T., van der Laan, S., Uglietti, C., Schibig, M. F., Neubert, R. E. M., Meijer, H. A. J., Brand, W. A., Jordan, A., Richter, J. M., Rothe, M., and Leuenberger, M. C.: Atmospheric CO_2, $\delta(O_2/N_2)$ and $\delta^{13}CO_2$ measurements at Jungfraujoch, Switzerland: results from a flask sampling intercomparison program, Atmos. Meas. Tech., 6, 1805-1815, 10.5194/amt-6-1805-2013, 2013.

Vigouroux, C., Blumenstock, T., Coffey, M., Errera, Q., García, O., Jones, N. B., Hannigan, J. W., Hase, F., Liley, B., Mahieu, E., Mellqvist, J., Notholt, J., Palm, M., Persson, G., Schneider, M., Servais, C., Smale, D., Thölix, L. and De Mazière, M.: Trends of ozone total columns and vertical distribution from FTIR observations at eight NDACC stations around the globe, Atmospheric Chemistry and Physics, 15(6), 2915–2933, doi:10.5194/acp-15-2915-2015, 2015.

Wunch, D., Toon, G. C., Blavier, J.-F. L., Washenfelder, R. A., Notholt, J., Connor, B. J., Griffith, D. W. T., Sherlock, V., and Wennberg, P. O.: The Total Carbon Column Observing Network, Philosophical Transactions of the Royal Society of London A: Mathematical, Physical and Engineering Sciences, 369, 2087-2112, 10.1098/rsta.2010.0240, 2011.

Yokota, T., Yoshida, Y., Eguchi, N., Ota, Y., Tanaka, T., Watanabe, H., and Maksyutov, S.: Global Concentrations of CO_2 and CH_4 Retrieved from GOSAT: First Preliminary Results, SOLA, 5, 160-163, 10.2151/sola.2009-041, 2009.

1   Zander, R., Mahieu, E., Demoulin, P., Duchatelet, P., Roland, G., Servais, C., Mazière, M. D.,

2   Reimann, S., and Rinsland, C. P.: Our changing atmosphere: Evidence based on long-term

3   infrared solar observations at the Jungfraujoch since 1950, Science of The Total Environment,

4   391, 184-195, http://dx.doi.org/10.1016/j.scitotenv.2007.10.018, 2008.

5   Zellweger, C., Ammann, M., Buchmann, B., Hofer, P., Lugauer, M., Rüttimann, R., Streit, N.,

6   Weingartner, E., and Baltensperger, U.: Summertime NO y speciation at the Jungfraujoch,

7   3580 m above sea level, Switzerland, Journal of Geophysical Research: Atmospheres, 105,

8   6655-6667, 10.1029/1999JD901126, 2000.

9   Zellweger, C., Forrer, J., Hofer, P., Nyeki, S., Schwarzenbach, B., Weingartner, E., Ammann,

10   M., and Baltensperger, U.: Partitioning of reactive nitrogen (NOy) and dependence on

11   meteorological conditions in the lower free troposphere, Atmos. Chem. Phys., 3, 779-796,

12   10.5194/acp-3-779-2003, 2003.

13   Zellweger, C., Hüglin, C., Klausen, J., Steinbacher, M., Vollmer, M., and Buchmann, B.:

14   Inter-comparison of four different carbon monoxide measurement techniques and evaluation

15   of the long-term carbon monoxide time series of Jungfraujoch, Atmos. Chem. Phys., 9, 3491-

16   3503, 10.5194/acp-9-3491-2009, 2009.

17   Zeng, N., Zhao, F., Collatz, G. J., Kalnay, E., Salawitch, R. J., West, T. O., and Guanter, L.:

18   Agricultural Green Revolution as a driver of increasing atmospheric CO_2 seasonal amplitude,

19   Nature, 515, 394-397, 10.1038/nature13893, 2014.
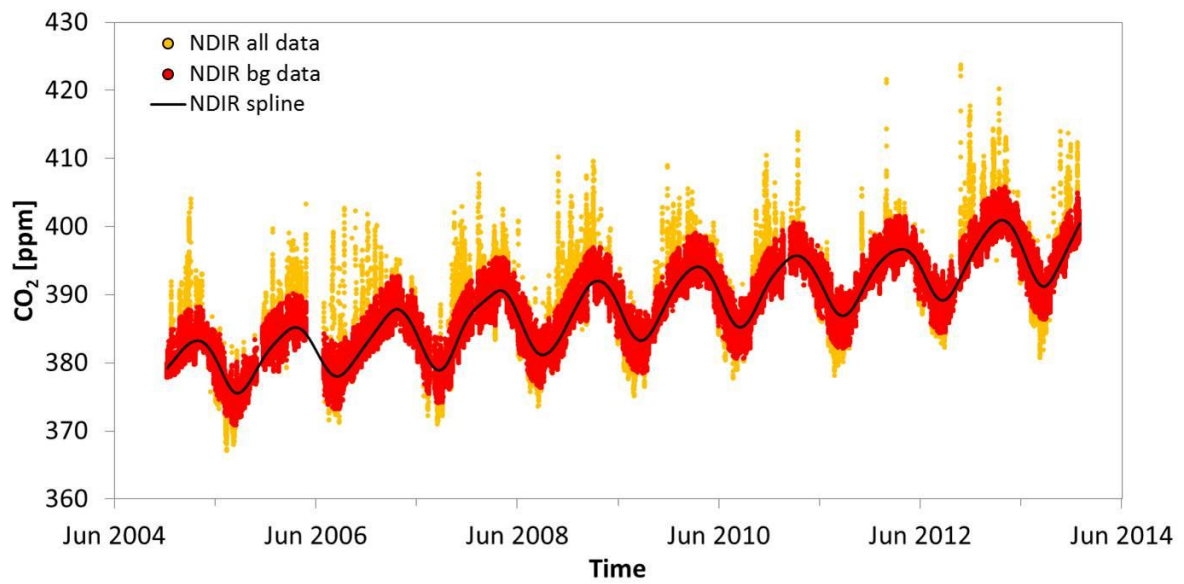
2   Figure 1. In-situ CO_2 mole fractions of the NDIR measurements as a function of time in ppm

3   at JFJ: All hourly averages before filtering (yellow), hourly averages after filtering (red) and

4   the spline (black line). Note that the yellow points correspond to only about 5 % of the whole

5   dataset.
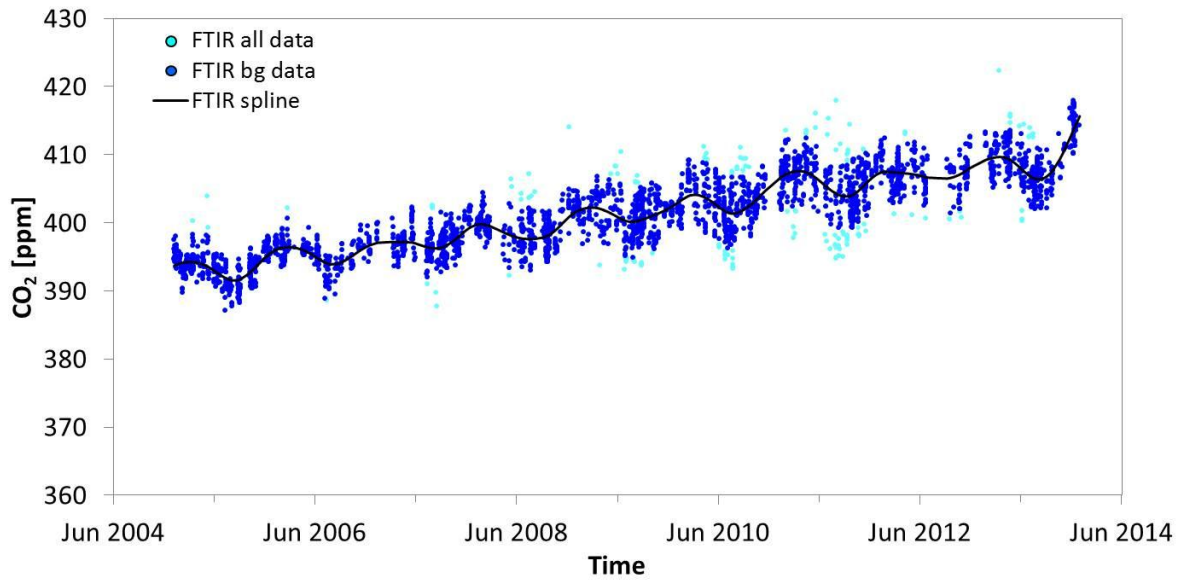
2 Figure 2. CO$_2$ mole fractions of the FTIR measurements as a function of time in ppm in the

3 column above JFJ: All hourly averages before filtering (light blue), hourly averages after

4 filtering (dark blue) and the spline (black line). The light blue points correspond to about 5 %

5 of the whole dataset.
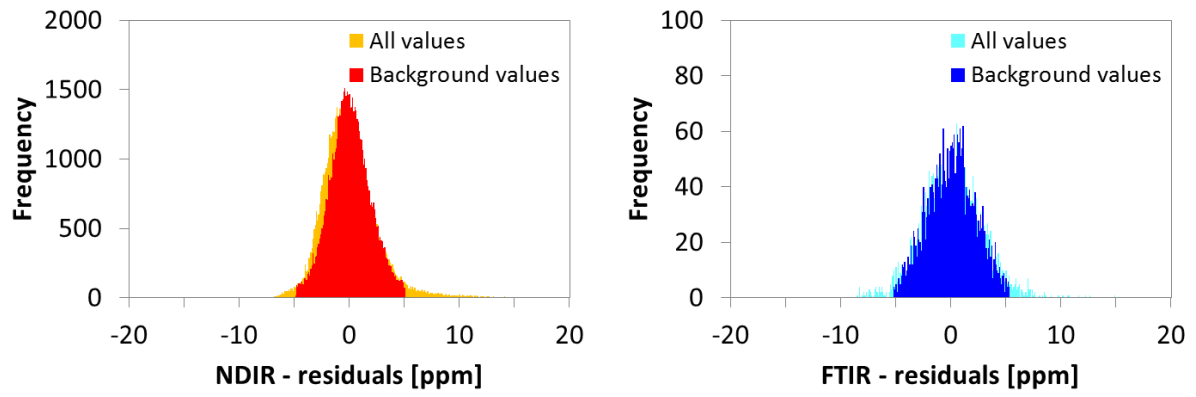
Figure 3. A: Histogram of all NDIR residuals (yellow) and the filtered NDIR residuals representing the background values (red) of the in-situ measurements; B: Histogram of all FTIR residuals (light blue) and the filtered FTIR residuals representing the background values (blue) of the column.
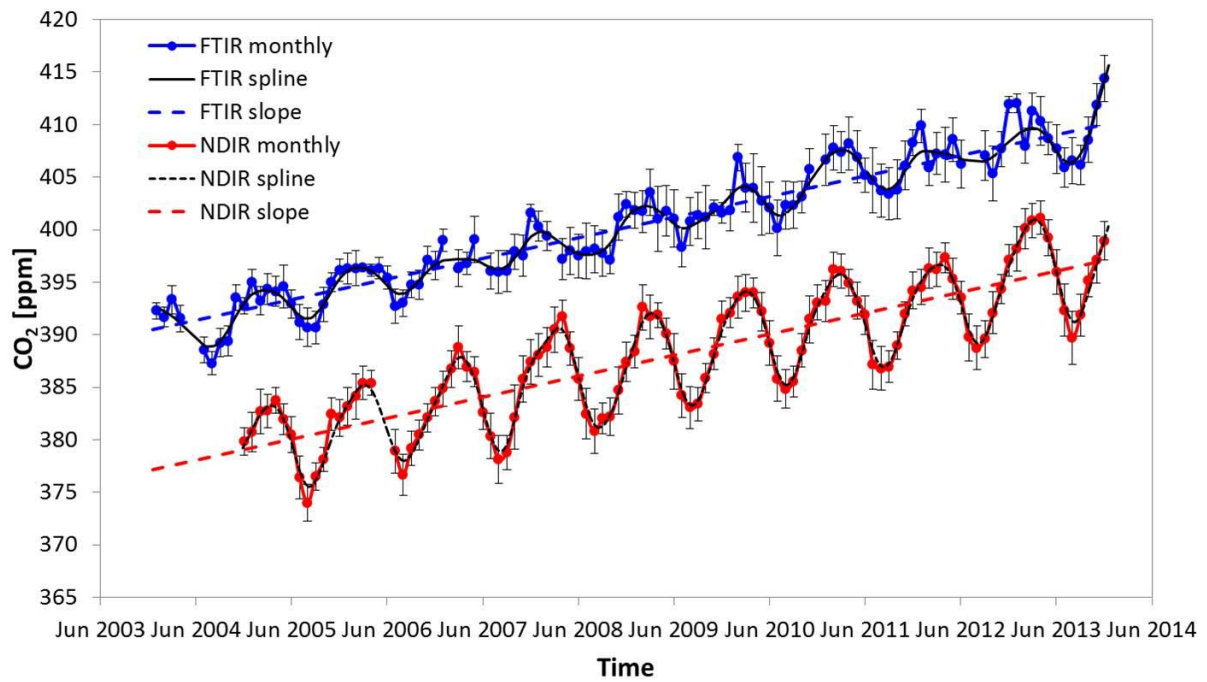
2   Figure 4. FTIR and NDIR CO_2 measurements at JFJ as a function of time: Monthly averages

3   of the filtered FTIR data (blue), spline (black line), the annual CO_2 increase calculated from

4   the filtered FTIR dataset (blue dashed line), monthly averages of the filtered NDIR data (red),

5   spline (black dotted line) and the annual CO_2 increase calculated from the filtered NDIR

6   dataset (red dashed line).
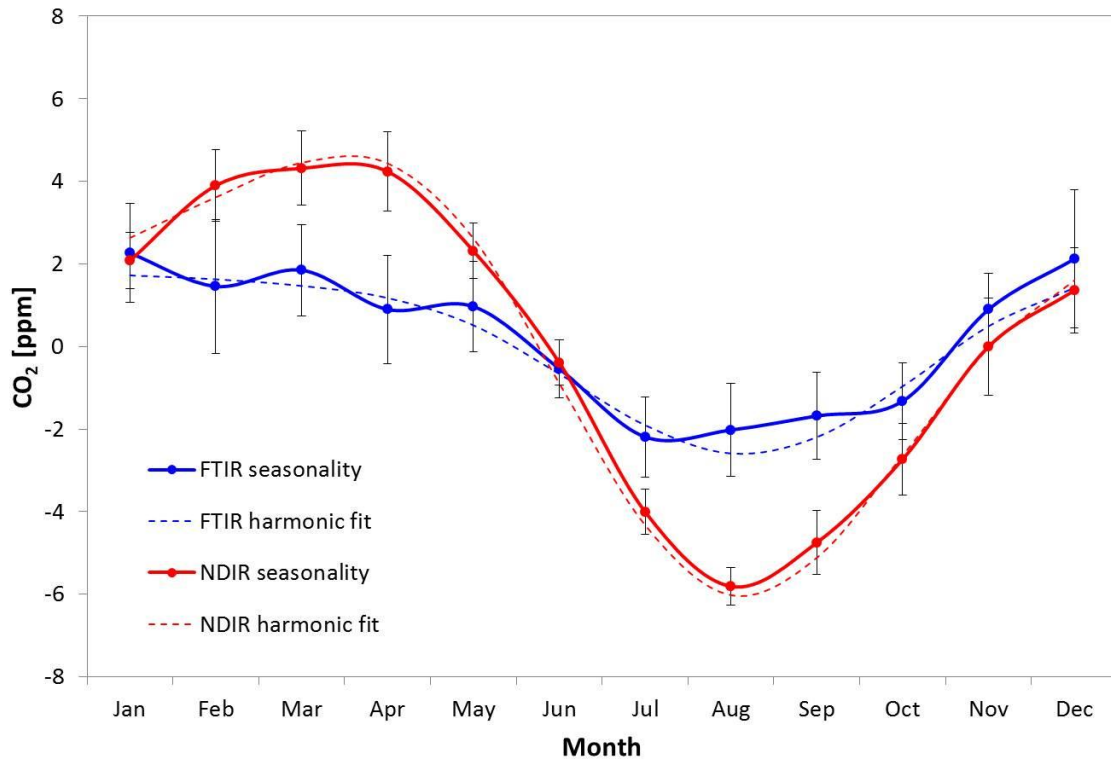
2 Figure 5. Monthly averaged seasonality of the filtered FTIR and NDIR CO_2 measurements for

3 the nine years of the comparison: averaged NDIR seasonality (red), two harmonic fit of the

4 NDIR seasonality (red dashed line), averaged FTIR seasonality (blue) and two harmonic fit of

5 the FTIR seasonality (dashed blue line).
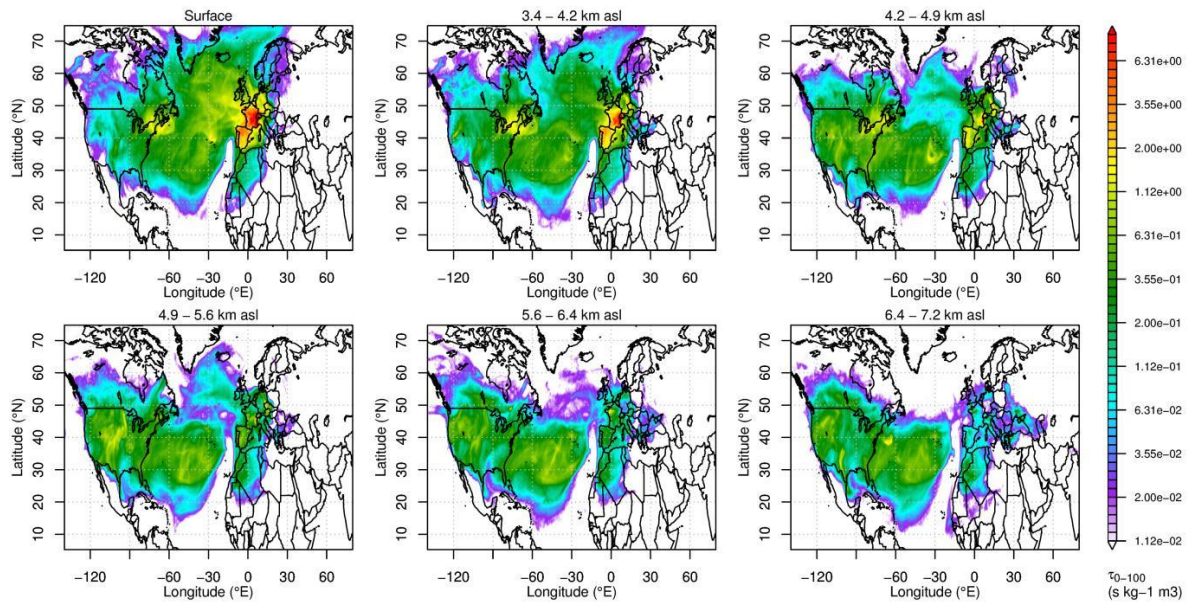
2 Figure 6. Surface source sensitivity (footprints) of the air masses at JFJ (surface in-situ) and in

3 the sub-columns above JFJ in August (CO_2 minimum of FTIR and NDIR time series) in the

4 period 2009 to 2011 simulated with FLEXPART. The height of the sub-columns is given

5 above the according subplots, the x-axis is the longitude, the y-axis represents the latitude, the

6 color code of the sensitivity is given at the right side.
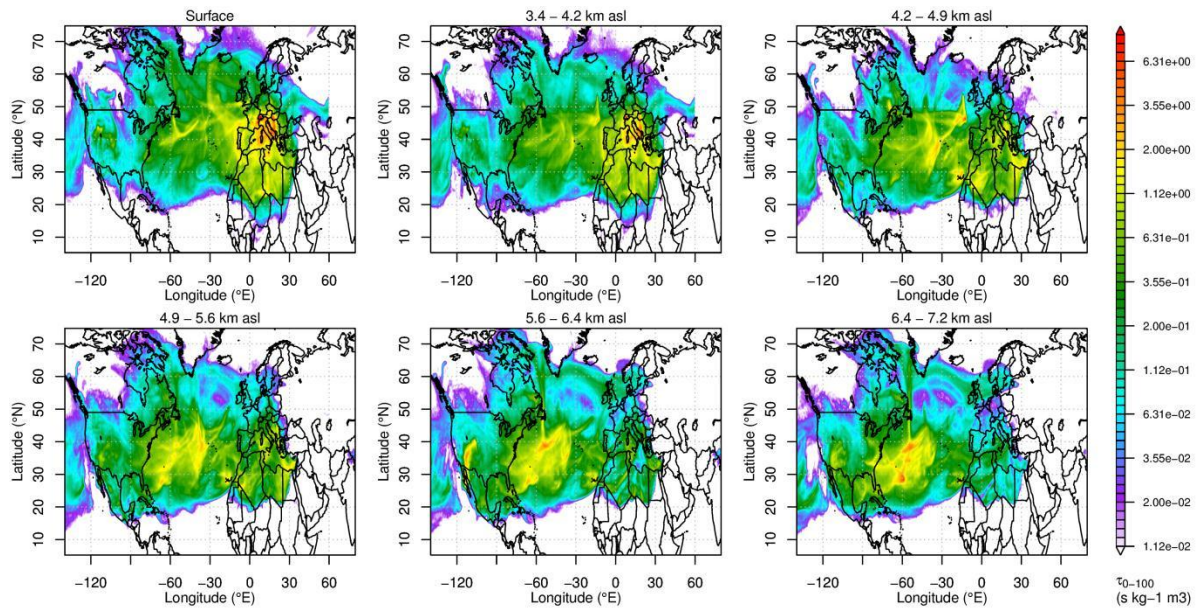
Figure 7. Surface source sensitivity (footprints) of the air masses at JFJ (surface in-situ) and in the sub-columns above JFJ in January (CO_2 maximum of the FTIR dataset) in the period 2009 to 2011 simulated with FLEXPART. The height of the sub-columns is given above the according subplots, the x-axis is the longitude, the y-axis represents the latitude, the color code of the sensitivity is given at the right side.
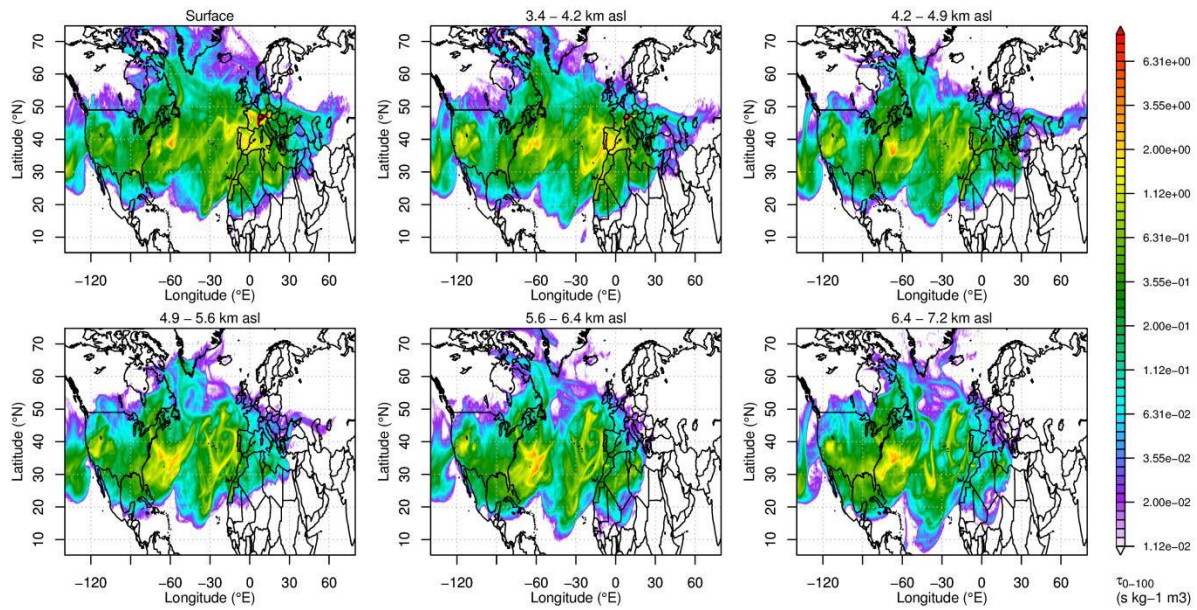
Figure 8. Surface source sensitivity (footprints) of the air masses at JFJ (surface in-situ) and in the sub-columns above JFJ in March (CO_2 maximum of the NDIR dataset) in the period 2009 to 2011 simulated with FLEXPART. The height of the sub-columns is given above the according subplots, the x-axis is the longitude, the y-axis represents the latitude, the color code of the sensitivity is given at the right side.
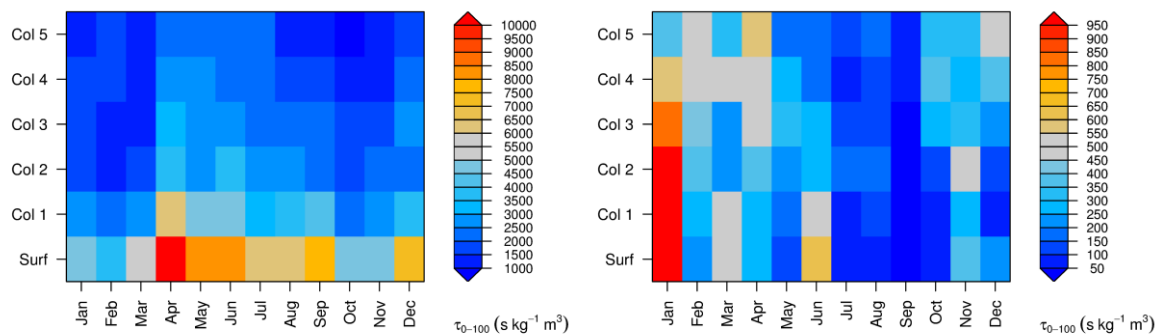
Figure 9, Annual cycle of FLEXPART derived total surface residence time over land for different vertical arrival columns above Jungfraujoch: (left) for land surfaces north of 30°N and (right) for land surfaces south of 30°N.
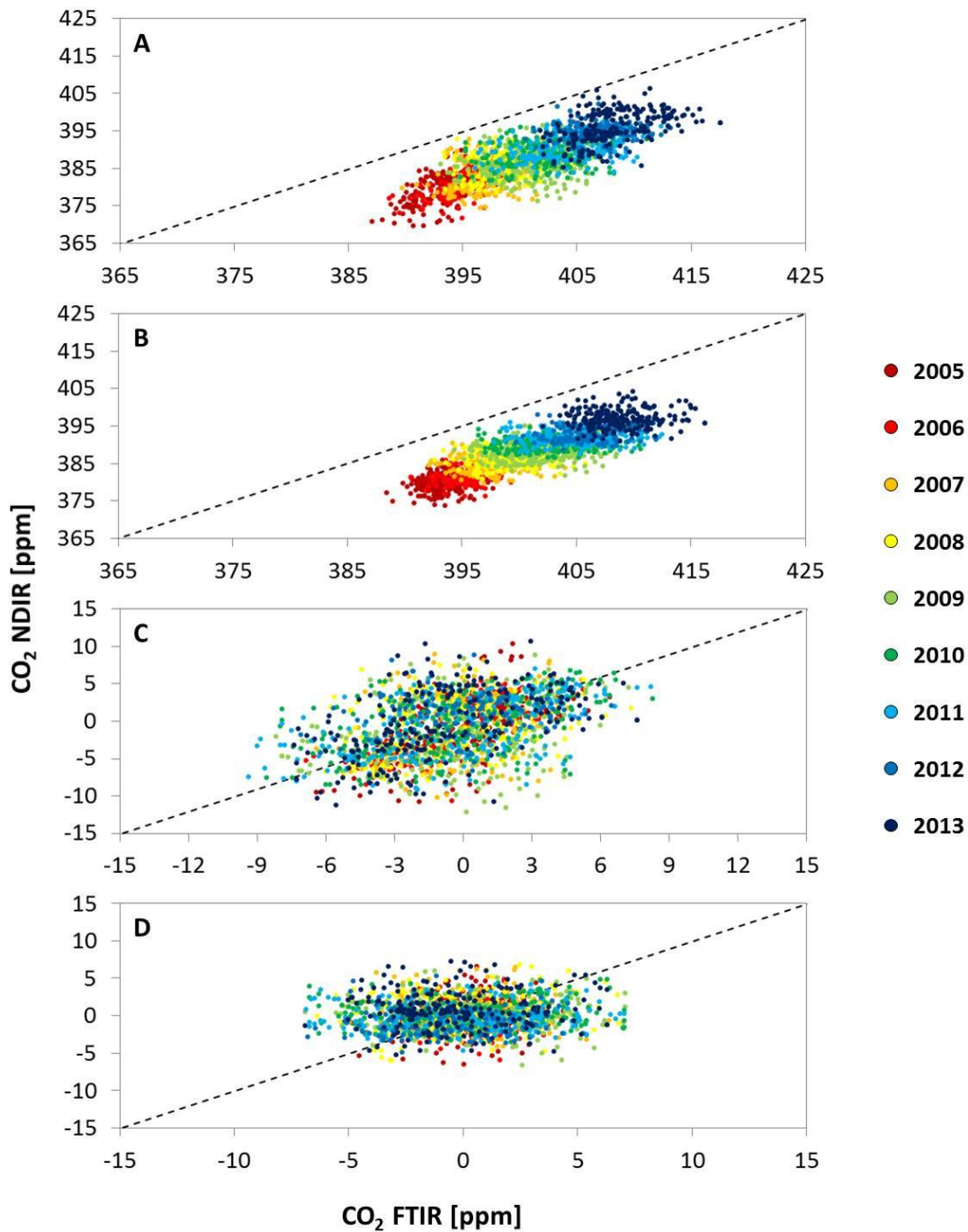
Figure 10. Correlation plots of the filtered hourly NDIR CO_2 measurements vs. the filtered
FTIR CO_2 measurements. The different colors refer to the years 2005 to 2013 (see legend). A:
The NDIR CO_2 measurements vs. FTIR CO_2 measurements including both, the annual CO_2
increase and the seasonality; B: As A but without seasonality; C: As A but detrended; D: As
A but with neither annual CO_2 increase nor seasonality. The dashed line is the 1:1 line.
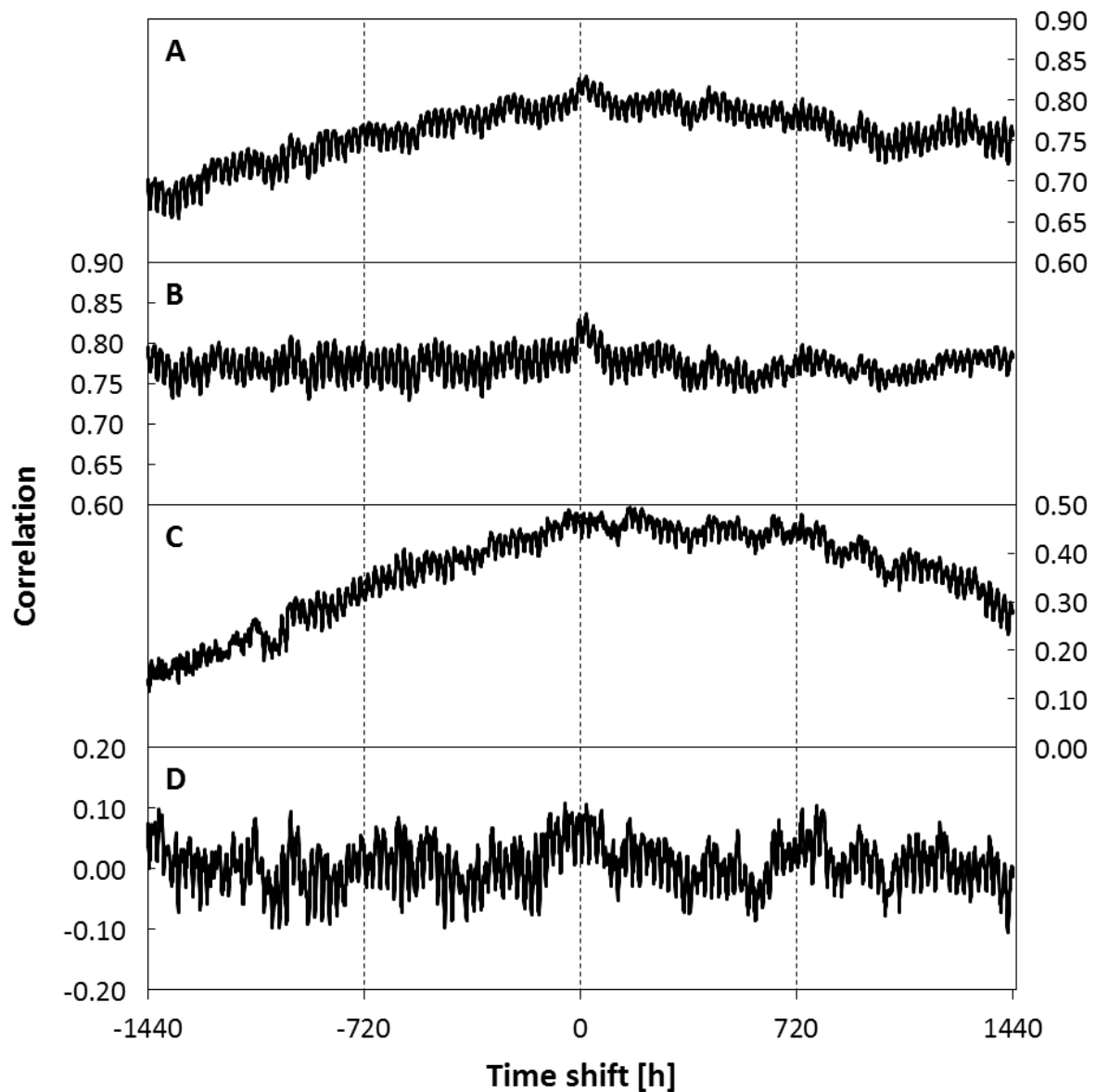
Figure 11. Evolution of the correlation between the filtered FTIR and NDIR datasets with changing time shift. A: Correlation between complete datasets; B: Correlation between the two datasets without seasonality; C: Correlation between the two datasets without trend; D: Correlation between the two datasets with neither trend nor seasonality.
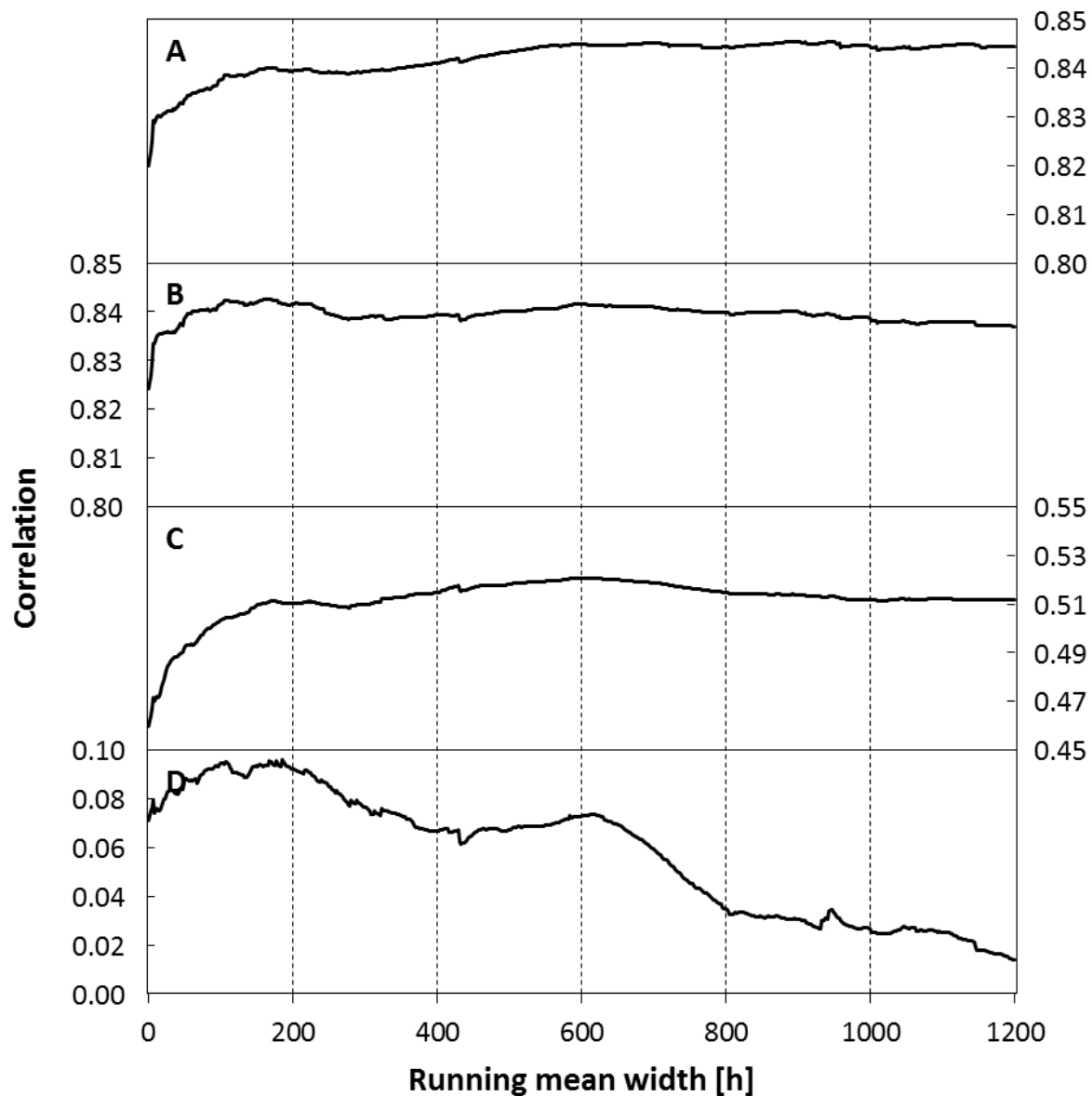
Figure 12. Change of the correlation between the filtered FTIR and NDIR datasets with
increasing width of the running mean. A: Correlation between the two datasets with
seasonality and slope; B: Correlation between the two datasets without seasonality; C:
Correlation between the two datasets without slope; D: Correlation between the two datasets
with neither slope nor seasonality.
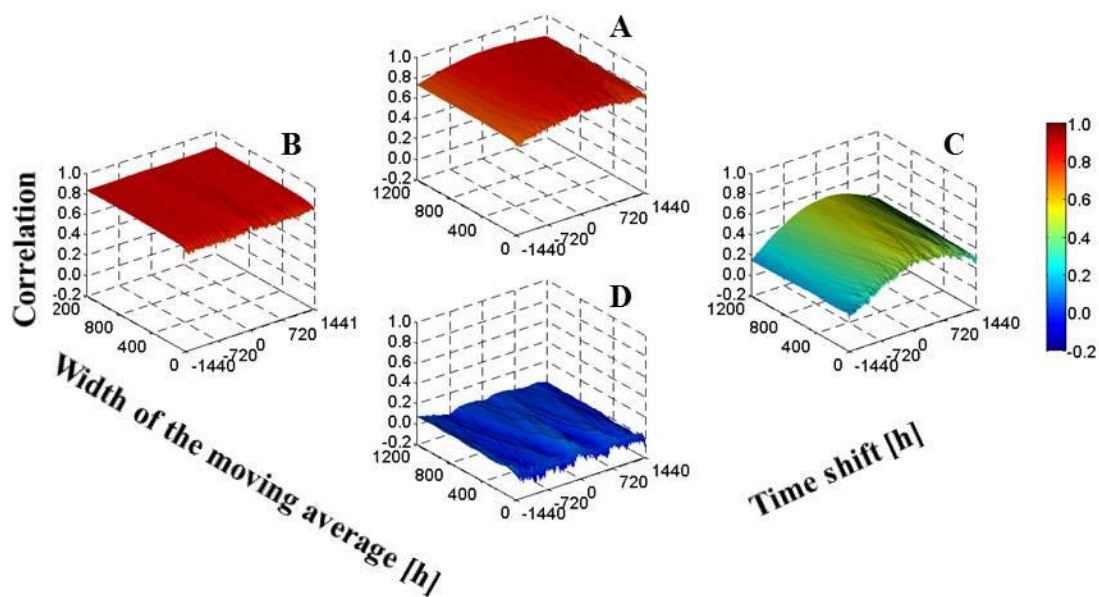
Figure 13. Surface plots of the correlation of the NDIR CO_2 measurements vs. the FTIR CO_2 measurements. The x-axis corresponds to the time shift, the y-axis to the width of the moving average and the z-axis to the correlation between the FTIR and the NDIR dataset, the color code illustrates the correlation and corresponds to the z-axis values. A: The FTIR CO_2 measurements vs. the corresponding NDIR CO_2 measurements including the annual CO_2 increase as well as the seasonality; B: As A but without seasonality; C: As A but detrended; D: As A but detrended and deseasonalized.